Acta Mech 228, 3483–3495 (2017)
DOI 10.1007/s00707-017-1874-8

ORIGINAL PAPER

H. B. Zhao · H. Feng · F. Liu · Y. W. Liu · P. H. Wen

Effect of nanoscale twin and dislocation pileup at twin boundary on crack blunting in nanocrystalline materials

Received: 18 November 2016 / Revised: 19 April 2017 / Published online: 17 June 2017

Abstract A theoretical model is developed to investigate the effects of the nanoscale twin and the dislocation pileup at the twin boundary on crack blunting in nanocrystalline materials. In the model, the nanoscale twin as a stress source approximately equals a quadrupole of wedge disclination. Using the complex variable method, the complex form expressions of the stress field and the force field are derived. The critical stress intensity factors (SIFs) for the first dislocation emission from the crack tip are calculated. The effects of the dislocation pileup, disclination strength, twin size, twin orientation, twin position and crack length on the critical SIFs are discussed in detail. Moreover, the shielding/anti-shielding effect produced by the twin, the dislocation pileup at the twin boundary and the first dislocation emitted on the crack tip is discussed. The results show that both the twin and the dislocation pileup at the twin boundary would suppress the dislocation emission from the crack tip. The suppressive effect induced by the dislocation pileup at the twin boundary is much stronger that that by the twin. Meanwhile, the emission angle has a significant effect on the mode I shielding/anti-shielding effect on the crack tip a.

1 Introduction

Nanocrystalline materials have attracted much attention due to their unique mechanical characteristics [1–5]. In most cases, nanocrystalline materials exhibit superior strength, strong hardness and good wear resistance, but at the expense of low tensile ductility and fracture toughness, which considerably limits their practical application [4,5]. However, some nanocrystalline materials with good tensile ductility of enhanced toughness have been studied and reported. The outstanding combination of good ductility and superior strength has created high interest in understanding the toughening mechanisms specific to nanocrystalline materials. Recently, various models have been developed to explain this phenomenon. In most of them, local migration of grain boundaries [6], rotational deformation [7,8], grain boundary sliding [9] and deformation twinning [10,11] have been theoretically described as specific deformation models in nanocrystalline materials.

The behaviors of twins, particularly nucleation, growth and interaction are contributing to the hardening of nanocrystalline materials [12–15]. Several studies have reported the mechanical behaviors of deformation twins in Magnesium and Zirconium. Romanov and Vladimirov [16] have proposed that the deformation twin as a

H. B. Zhao · H. Feng (✉) · Y. W. Liu
State Key Laboratory of Advanced Design and Manufacturing for Vehicle Body, Hunan University, Changsha 410082, China
E-mail: huifeng2010s@gmail.com

F. Liu
State Key Laboratory of Power Metallurgy, Central South University, Changsha 410083, China

P. H. Wen
School of Engineering and Material Science, Queen Mary, University of London, London, UK

stress source can be simulated by a disclination quadrupole. Feng et.al [17] have suggested a theoretical model to describe the dislocation-mediated mechanisms for the nucleation and growth of nanoscale deformation twin in hexagonal-close-packed materials. According to the theory of dislocations [18], the generation of the nanotwin *ABCD* is accompanied by the formation of a quadrupole of $\pm\Omega$ disclinations, whose stress field affects the further growth of the crack.

For nanotwinned materials, submicron-sized grains are subdivided into nanometer-thick twin/matrix lamellar structure by the twin boundaries (TBs) [10,19–22], so there are many twin boundaries–grain boundaries (TBs–GBs) as shown in Fig. 1b. When dislocations glide parallel to the TBs, these dislocations do not experience any barrier until they are hindered by the GBs. With the deformation going ahead, dislocations begin to pile up at the twin boundary [23]. To study the influence of TBs, we assume that the emission of the first dislocation is followed by the emission of the further dislocation along the same slip plane. The new dislocation slip until it reaches its equilibrium position determined by the balance of the force exerted by the applied shear stress and the force exerted by the previously emitted dislocations [24].

Meanwhile, Ovid'ko and Sheinerman [24] have pointed out that if the stress intensity near the crack tip is large enough, the crack induces plastic shear through the emission of lattice dislocations from the crack tip. The emission of the dislocations from cracks causes effective blunting of cracks, and thus suppresses their growth and improves the toughness of nanocrystalline materials. Feng et al. [25] have established a grain size dependent model to describe the effect of a special physical micromechanism of plastic flow on the dislocation emission from an elliptical blunt crack tip in nanocrystalline solids. Fang et al. [26] have investigated the special rotational deformation on the emission of lattice dislocations from the crack tip. Fang et al. [27] have theoretically described the effect of cooperative grain boundary sliding and migration on emission of dislocations from a crack tip in nanocrystalline materials. Then, Ovid'ko et al. [28] have described the operation of the cooperative GB sliding and migration process near the tips of growing cracks and theoretically analyzed its effect on the fracture toughness of nanocrystalline materials.

In the above-mentioned works, the researchers have studied the effect of the special deformation models near the crack tip on the fracture toughness of the nanocrystalline materials. However, for nanotwinned materials, not only submicron-sized grains are subdivided into nanometer-thick twin/matrix lamellar structure by the twin boundaries, but also the dislocations begin to pile up at the twin boundary. Thus, the main work of this paper is to present a theoretical model to investigate the interaction between the twin, the dislocation pileup at the twin boundary and the crack. The effects of the dislocation pileup, disclination strength, twin size, twin orientation, twin position and crack length on SIFs at the crack tip are discussed. Moreover, the shielding/anti-shielding effect produced by the twin, the dislocation pileup at the twin boundary and the first dislocation emitted on the crack tip is discussed.

2 Model and problem formulation

Consider a deformed nanocrystalline solid with a flat crack of length l, under remote mode I and mode II loadings as shown in Fig. 1. For simplicity, the solid is modeled as an isotropic medium having the shear modulus μ and Poisson's ratio ν. The defect structure of the solid is assumed to be the same along the coordinate axis z perpendicular to the xy plane. This assumption will simplify the mathematical analysis of the problem, reducing it to the consideration of a two-dimensional structure.

Introduce a Cartesian system (x, y) and a polar coordinate system (r, θ) with the origin at the crack tip, as shown in Fig. 1b. In this model, the twin can be modeled as a disclination quadrupole *ABCD* [16], which consists of two positive disclinations with strength ω at $z_1 = r_1 e^{i\theta_1}$ and $z_3 = z_1 + de^{i\alpha} + se^{i(\alpha+\pi/2)}$ and two negative disclinations with the same strength at $z_2 = z_1 + de^{i\alpha}$ and $z_4 = z_1 + se^{i(\alpha+\pi/2)}$, respectively. Here, s and d represent the quadrupole arms (the twin size), α represents the angle between the crack and the twin boundary *AB* (*CD*). When dislocations glide parallel to TBs, these dislocations do not experience any barrier until they are hindered by GBs. With the deformation going ahead, dislocations begin to pile up at the twin boundary [29]. The number of the dislocations pileup at the twin boundary is assumed to be M.

For the plane strain problem, the stress field $(\sigma_{xx}, \sigma_{yy}, \sigma_{xy})$ and displacement field (μ_x, μ_y) can be expressed by two Muskhelishvili's complex potentials $\Phi(z)$ and $\Psi(z)$ in the complex plane $z = x + iy$ [30],

$$\sigma_{xx} + \sigma_{yy} = 2\left(\Phi(z) + \overline{\Phi(z)}\right), \tag{1}$$

$$\sigma_{xx} - i\sigma_{yy} = \Phi(z) + \overline{\Phi(z)} + z\overline{\Phi'(z)} + \overline{\Psi(z)}, \tag{2}$$

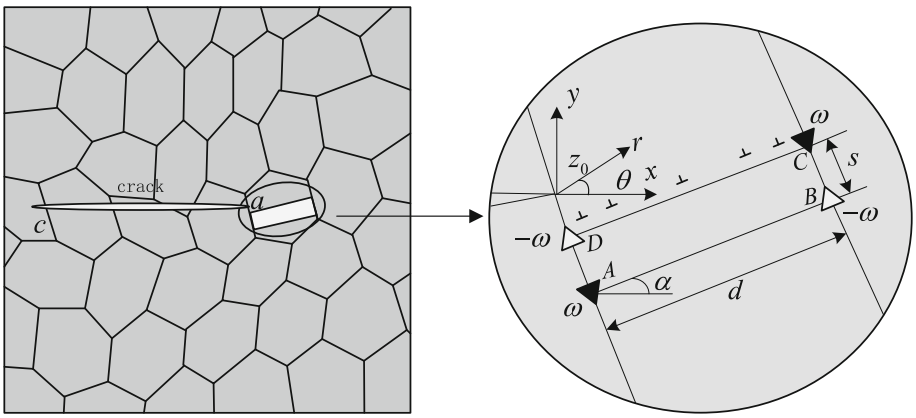

Fig. 1 Twin in a deformed nanocrystalline solid containing a flat crack. **a** General view and **b** magnified inset highlight the twin near the crack tip

$$2\mu(u'_x + u'_y) = (3-4\nu)\Phi(z) - \overline{\Phi(z)} - z\overline{\Phi'(z)} - \overline{\Psi(z)}, \tag{3}$$

where $u'_x = \partial u_x/\partial x$, $u'_y = \partial u_y/\partial y$, $\Phi'(z) = \mathrm{d}\,[\Phi(z)]/\mathrm{d}z$ and the over-bar represents the complex conjugate.

The stress field can be written as

$$\sigma_{xx} = \mathrm{Re}\left[2\Phi(z) - \bar{z}\Phi'(z) - \Psi(z)\right], \tag{4}$$

$$\sigma_{yy} = \mathrm{Re}\left[2\Phi(z) + \bar{z}\Phi'(z) + \Psi(z)\right], \tag{5}$$

$$\sigma_{xy} = \mathrm{Im}\left[\bar{z}\Phi'(z) + \Psi(z)\right]. \tag{6}$$

The boundary condition of the crack for the present problem can be expressed as

$$\sigma_{yy}(t) - i\sigma_{xy}(t) = 0, \quad t \in \text{crack}. \tag{7}$$

Firstly, consider the stress field produced by the dislocation pileup at the twin boundary *CD*. The dislocations are assumed to be of edge character, and the number of the dislocations at the TB *CD* is M. Referring to Fang et al. [27,30], the complex potentials $\Phi_b(z)$, $\Psi_b(z)$ and $\Omega_b(z)$ can be expressed as

$$\begin{aligned}\Phi_b(z) = {} & \frac{1}{2}\sum_{i=1}^{M}\left(\frac{w}{z-z_i} - \frac{w}{z-\bar{z}_i} - \frac{\bar{w}(z_i-\bar{z}_i)}{(z-\bar{z}_i)^2}\right) + \frac{1}{2\sqrt{(z-a)(z-c)}} \\ & \times \sum_{i=1}^{M}\left(\frac{w\sqrt{(z_i-a)(z_i-c)}}{z-z_i} + \frac{w\sqrt{(\bar{z}_i-a)(\bar{z}_i-c)}}{z-\bar{z}_i}\right. \\ & \left. + \frac{\bar{w}(z_i-\bar{z}_i)\sqrt{(\bar{z}_i-a)(\bar{z}_i-c)}}{(z-\bar{z}_i)^2} + \frac{\bar{w}\bar{z}_i(z_i-\bar{z}_i)}{(z-\bar{z}_i)\sqrt{(\bar{z}_i-a)(\bar{z}_i-c)}}\right),\end{aligned} \tag{8}$$

$$\begin{aligned}\Omega_b(z) = {} & \frac{1}{2}\sum_{i=1}^{M}\left(\frac{w}{z-z_i} - \frac{w}{z-\bar{z}_i} - \frac{\bar{w}(z_i-\bar{z}_i)}{(z-\bar{z}_i)^2}\right) - \frac{1}{2\sqrt{(z-a)(z-c)}} \\ & \times \sum_{i=1}^{M}\left(\frac{w\sqrt{(z_i-a)(z_i-c)}}{z-z_i} + \frac{w\sqrt{(\bar{z}_i-a)(\bar{z}_i-c)}}{z-\bar{z}_i}\right. \\ & \left. + \frac{\bar{w}(z_i-\bar{z}_i)\sqrt{(\bar{z}_i-a)(\bar{z}_i-c)}}{(z-\bar{z}_i)^2} + \frac{\bar{w}\bar{z}_i(z_i-\bar{z}_i)}{(z-\bar{z}_i)\sqrt{(\bar{z}_i-a)(\bar{z}_i-c)}}\right),\end{aligned} \tag{9}$$

$$\Psi_b(z) = -\Phi_b(z) - z\Phi'_b(z) - \overline{\Omega}_b(z), \tag{10}$$

where $w = \mu(b_y - ib_x)/4\pi(1-\nu)$.

With the substitution of Eqs. (8) and (10) into Eqs. (4)–(6), the stress field produced by the dislocation pileup at the twin boundary *CD* can be obtained.

Consider the stress field produced by the twin, which can be modeled as a wedge disclination quadrupole. Referring to Fang et al. [26], the complex potentials $\Phi_w(z)$ and $\Psi_w(z)$ have the following form:

$$\begin{aligned}\Phi_w(z) = {} & \frac{\mu\omega}{8\pi(1-\nu)}\left(\sum_{k=1}^{4}(-1)^{k+1}\ln\frac{z-z_k}{z-\bar{z}_k}-\sum_{k=1}^{4}(-1)^{k+1}\frac{z-z_k}{z-\bar{z}_k}\right)\\ & +\frac{\mu\omega}{8\pi(1-\nu)}X_0(z)\times\left(\sum_{k=1}^{4}(-1)^{k+1}\frac{1}{X_0(z_k)}\ln(z-z_k)\right.\\ & \left.-\sum_{k=1}^{4}(-1)^{k+1}(z_k-\bar{z}_k)-\sum_{k=1}^{4}(-1)^{k+1}\frac{1}{X_0(\bar{z}_k)}\left(\frac{z-z_k}{z-\bar{z}_k}+\ln(z-\bar{z}_k)\right)\right),\end{aligned} \tag{11}$$

$$\begin{aligned}\Psi_w(z) = {} & \frac{\mu\omega}{8\pi(1-\nu)}\left(\sum_{k=1}^{4}(-1)^{k+1}\left(\frac{3z-z_k}{z-\bar{z}_k}-\frac{\bar{z}_k}{z-z_k}\right)-\sum_{k=1}^{4}(-1)^{k+1}\frac{z(z-z_k)}{(z-z_k)^2}\right)\\ & \times\frac{\mu\omega}{8\pi(1-\nu)}X_0(z)\left(\sum_{k=1}^{4}(-1)^{k+1}\frac{1}{X_0(z_k)}\frac{\bar{z}_k}{z-z_k}+\sum_{k=1}^{4}(-1)^{k+1}\frac{1}{X_0(\bar{z}_k)}\right.\\ & \left.\times\left(\frac{z_k-3z}{z-\bar{z}_k}+\frac{z(z-z_k)}{(z-\bar{z}_k)^2}\right)\right)-\frac{\mu\omega}{8\pi(1-\nu)}X_0'(z)\left(\sum_{k=1}^{4}(-1)^{k+1}\frac{z}{X_0(z_k)}\right.\\ & \left.\times\ln(z-z_k)\quad-\sum_{k=1}^{4}(-1)^{k+1}z(z-\bar{z}_k)-\sum_{k=1}^{4}(-1)^{k+1}\frac{z}{X_0(\bar{z}_k)}\left(\frac{z-z_k}{z-\bar{z}_k}+\ln(z-\bar{z}_k)\right)\right),\end{aligned} \tag{12}$$

where $X_0(z)=1/\sqrt{(z-a)(z-c)}$ and $X_0'(z)=\mathrm{d}X_0(z)/\mathrm{d}z$.

With the substitution of Eqs. (11) and (12) into Eq. (4), the stress field due to the wedge disclination quadrupole can be obtained.

3 The emission force of lattice dislocations

When the stress intensity near the crack tip is large enough, the crack can induce plastic deformation through the emission of lattice dislocations from the crack tip [23,32–34]. For simplicity, we focus on the situation where the dislocations are of edge character and their Burgers vectors lie along the slip plane that makes an angle θ with the x-axis. The first dislocation is assumed to be located at $z_0 = r_0 e^{i\theta}$ in the coordination system. According to Fang et al. [27,31], the complex potentials of the first dislocation $\Phi_e(z)$, $\Omega_e(z)$ and $\Psi_e(z)$ can be expressed as follows:

$$\begin{aligned}\Phi_e(z) = {} & \frac{1}{2}\left(\frac{w}{z-z_0}-\frac{w}{z-\bar{z}_0}-\frac{\bar{w}(z_0-\bar{z}_0)}{(z-\bar{z}_0)^2}\right)+\frac{1}{2\sqrt{(z-a)(z-c)}}\\ & \times\left(\frac{w\sqrt{(z_0-a)(z_0-c)}}{z-z_0}+\frac{w\sqrt{(\bar{z}_0-a)(\bar{z}_0-c)}}{z-\bar{z}_0}\right.\\ & \left.+\frac{\bar{w}(z_0-\bar{z}_0)\sqrt{(\bar{z}_0-a)(\bar{z}_0-c)}}{(z-\bar{z}_0)^2}+\frac{\bar{w}\bar{z}_0(z_0-\bar{z}_0)}{(z-\bar{z}_0)\sqrt{(\bar{z}_0-a)(\bar{z}_0-c)}}\right),\end{aligned} \tag{13}$$

$$\begin{aligned}\Omega_e(z) = {} & \frac{1}{2}\left(\frac{w}{z-z_0}-\frac{w}{z-\bar{z}_0}-\frac{\bar{w}(z_0-\bar{z}_0)}{(z-\bar{z}_0)^2}\right)-\frac{1}{2\sqrt{(z-a)(z-c)}}\\ & \times\left(\frac{w\sqrt{(z_0-a)(z_0-c)}}{z-z_0}+\frac{w\sqrt{(\bar{z}_0-a)(\bar{z}_0-c)}}{z-\bar{z}_0}\right.\end{aligned}$$

$$+\frac{\bar{w}\left(z_0-\bar{z}_0\right)\sqrt{\left(\bar{z}_0-a\right)\sqrt{\left(\bar{z}_0-c\right)}}}{\left(z-\bar{z}_0\right)^2}+\frac{\bar{w}\bar{z}_0\left(z_0-\bar{z}_0\right)}{\left(z-\bar{z}_0\right)\sqrt{\left(\bar{z}_0-a\right)\sqrt{\left(\bar{z}_0-c\right)}}}\Bigg), \tag{14}$$

$$\Psi_e(z)=-\Phi_e(z)-z\Phi_e'(z)-\overline{\Omega}_e(z), \tag{15}$$

The force acting on the edge dislocation consists of four parts: the image force, the force produced by the dislocation pileup at the twin boundary, the force produced by the twin and the external force.

Firstly, the image force can be obtained as by Hirth and Lorth [18],

$$\begin{aligned} f_{\text{image}} &= f_x - if_y = \left[\tilde{\sigma}_{xy}(z_0)b_x+\tilde{\sigma}_{yy}(z_0)b_y\right]+i\left[\tilde{\sigma}_{xx}(z_0)b_x+\tilde{\sigma}_{xy}(z_0)b_y\right] \\ &= \frac{\mu b^2}{\pi(1+\kappa)}\left(\frac{\Phi_e^*(z_0)+\overline{\Phi_e^*(z_0)}}{w}+\frac{\bar{z}_0\Phi_e^{*\prime}(z_0)+\Psi_e^*(z_0)}{\bar{w}}\right), \end{aligned} \tag{16}$$

where $\tilde{\sigma}_{xx}$, $\tilde{\sigma}_{yy}$and $\tilde{\sigma}_{xy}$ are the components of the perturbation stress and

$$\Phi_e^*(z_0)=\lim_{z\to z_0}\left(\Phi_e(z)-\Phi_{e0}(z)\right), \tag{17}$$

$$\Phi_e^{*\prime}(z_0)=\lim_{z\to z_0}\frac{d\left(\Phi_e(z)-\Phi_{e0}(z)\right)}{dz}, \tag{18}$$

$$\Psi_e^*(z_0)=\lim_{z\to z_0}\left(\Psi_e(z)-\Psi_{e0}(z)\right), \tag{19}$$

where $\Phi_{e0}(z)=w/(z-z_0)$ and $\Psi_{e0}(z)=\bar{w}/(z-z_0)+w\bar{z}_0/(z-z_0)^2$.

Secondly, the force produced by the dislocation pileup at the twin boundary can be written as

$$\begin{aligned} f_{\text{boundary}} &= f_x - if_y = \left[\sigma_{bxy}(z_0)b_x+\sigma_{byy}(z_0)b_y\right]+1\left[\sigma_{bxx}(z_0)b_x+\sigma_{bxy}(z_0)b_y\right] \\ &= \frac{\mu b^2}{\pi(1+\kappa)}\left(\frac{\Phi_b(z_0)+\overline{\Phi_b(z_0)}}{w}+\frac{\bar{z}_0\Phi_b'(z_0)+\Psi_b(z_0)}{\bar{w}}\right), \end{aligned} \tag{20}$$

where σ_{bxx}, σ_{byy} and σ_{bxy} are the components of the stress field produced by the dislocation pileup at the twin boundary.

Thirdly, the force produced by the wedge disclination quadrupole (the twin) can be written as

$$\begin{aligned} f_{\text{wedge}} &= f_x - if_y = \left[\sigma_{xy}(z_0)b_x+\sigma_{yy}(z_0)b_y\right]+i\left[\sigma_{xx}(z_0)b_x+\sigma_{xy}(z_0)b_y\right] \\ &= \frac{\mu b^2}{\pi(1+\kappa)}\left(\frac{\Phi_w(z_0)+\overline{\Phi_w(z_0)}}{w}+\frac{\bar{z}_0\Phi_w'(z_0)+\Psi_w(z_0)}{\bar{w}}\right), \end{aligned} \tag{21}$$

where σ_{xx}, σ_{yy} and σ_{xy} are the components of the stress field produced by the wedge disclination quadrupole.

Lastly, the external force acting on the edge dislocation can be written as

$$f_\tau = b\sigma_{r\theta}=\frac{b}{\sqrt{2\pi r}}\left(\frac{1}{2}\sin\theta\cos\frac{\theta}{2}K_{\text{I}}^{\text{app}}+\left(\cos\frac{3\theta}{2}+\sin^2\frac{\theta}{2}\cos\frac{\theta}{2}\right)K_{\text{II}}^{\text{app}}\right), \tag{22}$$

where $K_{\text{I}}^{\text{app}}$ and $K_{\text{II}}^{\text{app}}$ are the generalized mode I and II SIFs produced by the remote loadings.

Then, the dislocation emission force can be written as,

$$\begin{aligned} f_{\text{emit}} &= f_x\cos\theta+f_y\sin\theta+f_\tau \\ &= Re\left[f_{\text{image}}+f_{\text{boundary}}+f_{\text{wedge}}\right]\cos\theta-\text{Im}\left[f_{\text{image}}+f_{\text{boundary}}+f_{\text{wedge}}\right]\sin\theta+f_\tau. \end{aligned} \tag{23}$$

With the substitution of Eqs. (16)–(22) into Eq. (23), we have the expression of the dislocation emission force.

4 The critical SIFs for the dislocation emission

A commonly accepted criterion for the emission of dislocations from the crack tip is that the force acting on them equals zero and the distance between the dislocation and the crack surface should be equal or larger than the dislocation core radius [37]. Combining the expressions (16)–(23) with the emission criterion $f_{\text{emit}} = 0$, the applied critical SIFs $K_{\text{IC}}^{\text{app}}$ and $K_{\text{IIC}}^{\text{app}}$ for the dislocation emission can be derived.

When $K_{\text{II}}^{\text{app}} = 0$,

$$K_{\text{IC}}^{\text{app}} = \frac{2\sqrt{2\pi r_0}}{b \sin\theta \cos\frac{\theta}{2}} \begin{pmatrix} \text{Im}\left[f_{\text{image}} + f_{\text{boundary}} + f_{\text{wedge}}\right] \sin\theta \\ -\text{Re}\left[f_{\text{image}} + f_{\text{boundary}} + f_{\text{wedge}}\right] \cos\theta \end{pmatrix},$$

and when $K_{\text{I}}^{\text{app}} = 0$,

$$K_{\text{IIC}}^{\text{app}} = \frac{\sqrt{2\pi r_0}}{b\left(\cos\frac{3\theta}{2} + \sin^2\frac{\theta}{2}\cos\frac{\theta}{2}\right)} \begin{pmatrix} \text{Im}\left[f_{\text{image}} + f_{\text{boundary}} + f_{\text{wedge}}\right] \sin\theta \\ -\text{Re}\left[f_{\text{image}} + f_{\text{boundary}} + f_{\text{wedge}}\right] \cos\theta \end{pmatrix},$$

where

$$f_{\text{image}} + f_{\text{wedge}} + f_{\text{boundary}} = \frac{\mu b^2}{\pi (1+\kappa)} \left[\frac{2Re\left[\Phi_e^*(z_0) + \Phi_w(z_0) + \Phi_b(z_0)\right]}{w} + \frac{\bar{z}_0 \left(\Phi_e^{*\prime}(z_0) + \Phi_w'(z_0) + \Phi_b'(z_0)\right) + \left(\Psi_e^*(z_0) + \Psi_w(z_0) + \Psi_b(z_0)\right)}{\bar{w}} \right].$$

Utilizing the expressions of the applied critical SIFs $K_{\text{IC}}^{\text{app}}$ and $K_{\text{IIC}}^{\text{app}}$, the effects of the twin and the dislocation pileup at the twin boundary on the dislocation emission from the crack tip can be analyzed. The normalized critical SIFs are defined as $K_{\text{IC}}^0 = K_{\text{IC}}^{\text{app}}/(\mu\sqrt{b})$ and $K_{\text{IIC}}^0 = K_{\text{IIC}}^{\text{app}}/(\mu\sqrt{b})$. The disclination strengths are denoted as $\pm\omega$ and the position of the first dislocation $r_0 = b/2$. The quadrupole arms are assumed to be much smaller compared to the crack length l. The following typical values of parameters for the nanocrystalline material 3C–SiC are used, $\mu = 217$ GPa and $\nu = 0.23$ [38].

Firstly, the crack length in the nanocrystalline solid is assumed to be $l = 100$ nm and the Burgers vector of the edge dislocation at the crack tip is $b = 0.25$ nm. The variations of the normalized critical SIFs K_{C}^0 and K_{C}^p (without considering the effect of the dislocation pileup at the twin boundary) with the disclination strength ω are depicted in Fig. 2. It can be found that the normalized critical SIFs K_{IC}^0 and K_{IIC}^0 both increase with the increment of disclination strength ω. The critical SIFs have the smallest values when the twin and the dislocation pileup at the twin boundary do not exist. In addition, when the effect of the dislocation pileup at the twin boundary is considered, the values of the critical SIFs are about two times larger than those under the situation that the dislocation pileup at the twin boundary is not considered. This phenomenon indicates that the twin and the dislocation pileup at the twin boundary release, in part, the high stresses near the crack tip

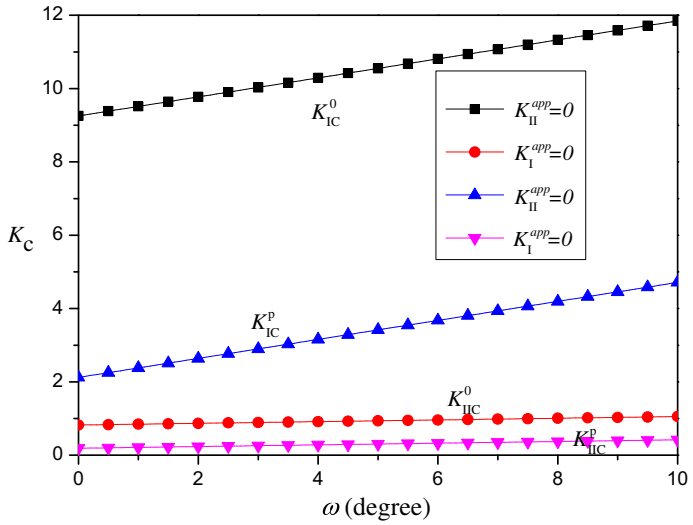

Fig. 2 Dependence of the critical normalized SIFs K_{C}^0 and K_{C}^p (without considering the effect of the dislocation pileup at twin boundary) on the disclination strength ω ($\alpha = \pi/6$, $r_1 = 0.1$ nm, $\theta_0 = 10°$, $\theta_1 = 0°$, $d = 15$ nm and $s = 3$ nm)

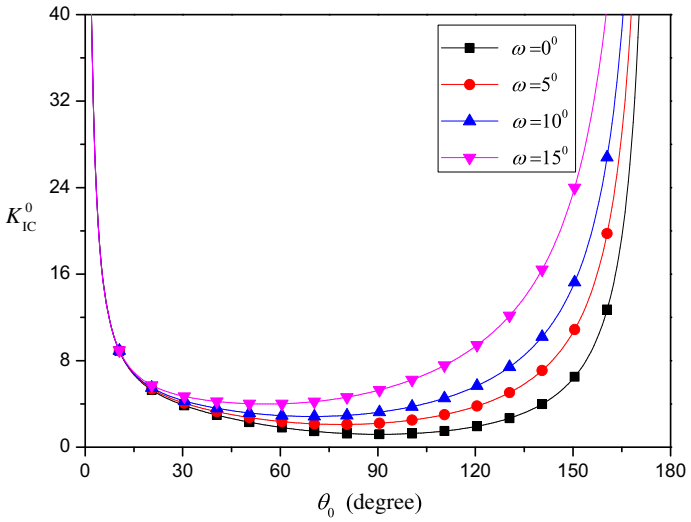

Fig. 3 Dependence of the critical normalized SIFs K^0_{IC} on the edge dislocation emission angle θ_0 with different ω ($\alpha = \pi/6$, $r_1 = 0.1$ nm, $\theta_1 = 0°$, $d = 15$ nm and $s = 3$ nm)

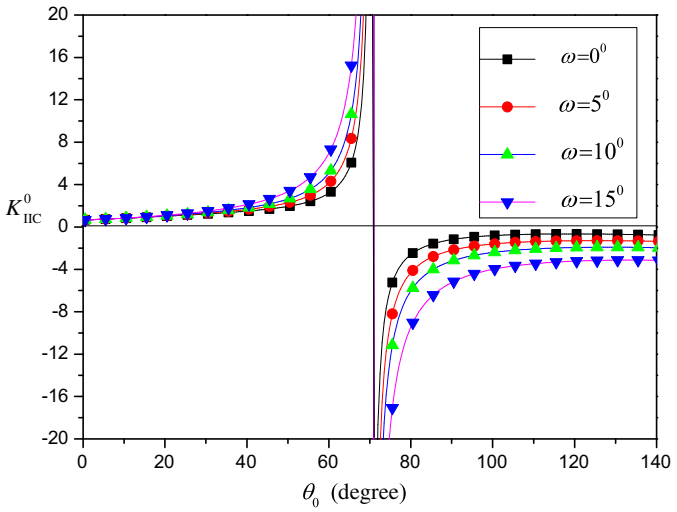

Fig. 4 Dependence of the critical normalized SIFs K^0_{IIC} on the edge dislocation emission angle θ_0 with different ω ($\alpha = \pi/6$, $r_1 = 0.1$ nm, $\theta_1 = 0°$, $d = 15$ nm and $s = 3$ nm)

area and therefore enhance the critical SIFs for dislocation emission. When the strength of the twin is higher, the edge dislocation is more difficult to emit from the crack tip. It can be also found that when the disclination strength is certain, K^0_{IIC} is much smaller than K^0_{IC}, which means that the mode II loadings are much easier than the mode I loadings to emit the dislocations from the crack tip.

Figures 3 and 4 show the normalized critical SIFs K^0_C for dislocation emission as functions of emission angle θ_0 with difference disclination strength ω for mode I and II applied loadings. For the model I critical SIFs in Fig. 3, they decrease from infinity to minimums and then increase with increasing emission angle. When $\omega = 0°$, the most probable angle θ_{min} for the dislocation emission is 90.5° The most probable emission angle decreases with the increment of disclination strength ω. For $\omega = 5°$, the most probable emission angle $\theta_{min} = 78°$; for $\omega = 10°$, $\theta_{min} = 70°$; and for $\omega = 15°$, $\theta_{min} = 53°$. However, the normalized critical mode II SIFs in Fig. 4 increase from a finite positive value to infinity with the increment of edge dislocation emission angle, then switch to negative value. Referring to the work by Huang and Li [39], the sign of the SIFs can be determined by the direction of the Burgers vector of the emerging dislocations. So the most probable emission angle for the positive edge dislocation is always zero under the mode II loading. And when the influence of the twin is ignored ($\omega = 0°$), the most probable angle for the negative edge dislocation emission is 119°.

The dependence of the normalized critical SIFs K^0_{IC} on the twin size d with different twin orientation angles α are depicted in Fig. 5. It can be seen that the normalized critical SIFs K^0_{IC} decrease with increasing twin size

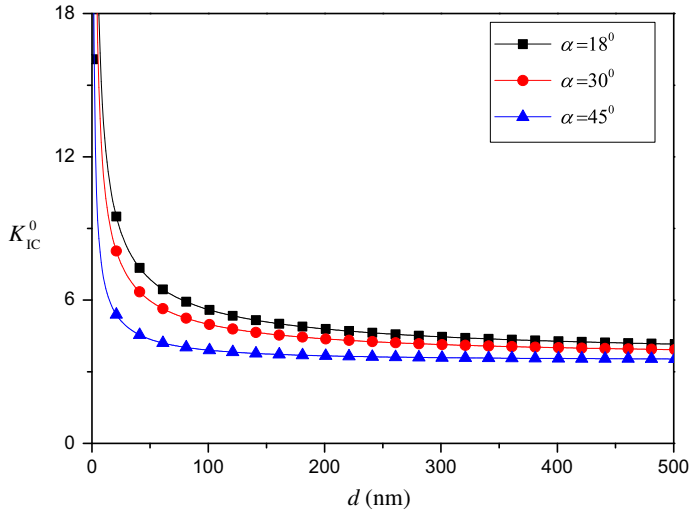

Fig. 5 Dependence of the critical normalized SIFs K_{IC}^{0} on the twin size d with different α ($\omega = \pi/72$, $r_1 = 0.1$ nm, $\theta_0 = 10°$, $\theta_1 = 0°$ and $s = 3$ nm)

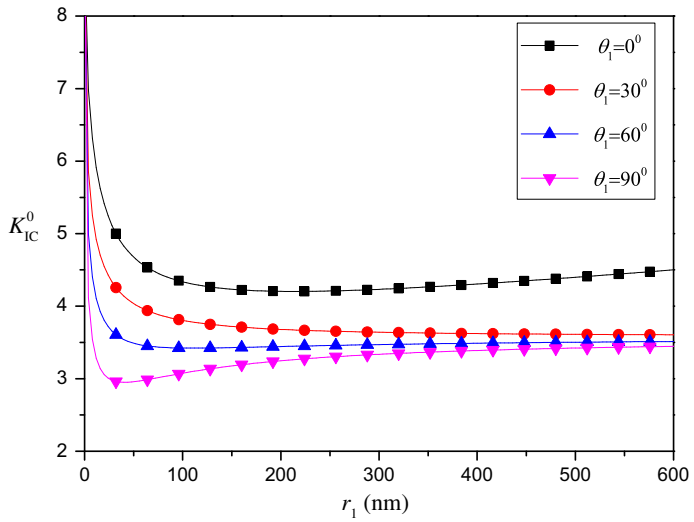

Fig. 6 Dependence of the critical normalized SIFs K_{IC}^{0} on the disclination position r_1 with different θ_1 ($\alpha = \pi/3$, $\omega = \pi/72$, $\theta_0 = 10°$, $d = 15$ nm and $s = 3$ nm)

d and the angle α. The effect of the twin position (r_1 and θ_1) on the normalized critical SIFs K_{IC}^{0} is shown in Fig. 6. It can be seen that the normalized critical SIFs K_{IC}^{0} decrease dramatically and then increase slightly with an increment of the twin position parameter r_1 and decrease with increasing angle θ_1. This indicates that the location of the twin has a significant influence on the dislocation emission from the crack tip. Under a certain condition, there is a best twin position which can make the dislocation emission easiest.

Then, the variation of the normalized critical SIF K_{IC}^{0} with the crack length is depicted in Fig. 7. The normalized critical SIF K_{IC}^{0} decreases with increasing crack length, and then tends to a constant value. Hence, the shorter crack tends to grow, but the longer crack is easier to be blunted.

5 The anti-shielding effect and shielding effect

According to the definition of the SIF, the expression of the SIFs at the crack tip a and c of a limited crack can be derived as [11,40,41]

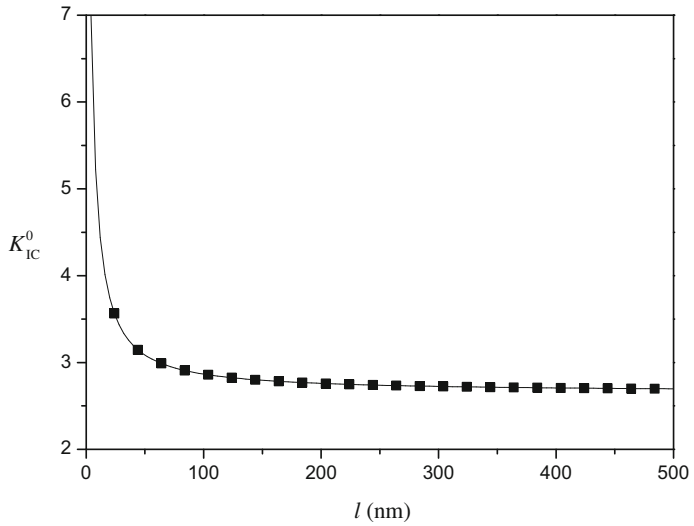

Fig. 7 Dependence of the critical normalized SIFs K_{IC}^{0} on the crack length l ($\alpha = \pi/3$, ω=$\pi/72$, $r_0 = 0.125$ nm, $r_1 = 0.1$ nm, $\theta_0 = 10°$, $d = 15$ nm and $s = 3$ nm)

$$K^c = K_1^c - iK_{II}^c = 2\sqrt{2\pi}\lim_{z\to c}\left[\sqrt{z-a}\phi(z)\right],$$
$$K^a = K_1^a - iK_{II}^a = 2\sqrt{2\pi}\lim_{z\to a}\left[\sqrt{z-a}\phi(z)\right]. \tag{24}$$

The SIFs due to the twin, the first dislocation emitted from the crack tip [3,42] and the dislocation pileup at the twin boundary [27] can be obtained, respectively, as

$$\begin{aligned} K_I^q - iK_{II}^q = {} & \frac{\mu\omega}{2\sqrt{2\pi}(1-\nu)}\frac{1}{\sqrt{c-a}} \\ & \times\left(\sum_{k=1}^{4}(-1)^{k+1}\sqrt{(z_k-a)(z_k-c)}\ln(c-z_k) - \sum_{k=1}^{4}(-1)^{k+1}(z_k-\bar{z}_k)\right. \\ & \left.-\sum_{k=1}^{4}(-1)^{k+1}\sqrt{(\bar{z}_k-a)(\bar{z}_k-c)}\left(\frac{c-z_k}{c-\bar{z}_k}-\ln(c-\bar{z}_k)\right)\right), \end{aligned} \tag{25}$$

$$\begin{aligned} K_I^d - iK_{II}^d = {} & \frac{\mu b}{2\sqrt{2\pi}(1-\nu)}\frac{1}{\sqrt{c-a}}\left(\frac{(\sin\theta - i\cos\theta)\sqrt{(z_0-a)(z_0-c)}}{c-z_0}\right. \\ & +\frac{(\sin\theta + i\cos\theta)\bar{z}_0(z_0-\bar{z}_0)}{(c-\bar{z}_0)\sqrt{(\bar{z}_0-a)(\bar{z}_0-c)}} + \frac{(\sin\theta - i\cos\theta)\sqrt{(\bar{z}_0-a)(\bar{z}_0-c)}}{c-\bar{z}_0} \\ & \left.+\frac{(\sin\theta + i\cos\theta)(z_0-\bar{z}_0)\sqrt{(\bar{z}_0-a)(\bar{z}_0-c)}}{(c-\bar{z}_0)^2}\right), \end{aligned} \tag{26}$$

$$\begin{aligned} K_I^b - iK_{II}^b = {} & \sum_{i=1}^{M}\frac{\mu b}{2\sqrt{2\pi}(1-\nu)}\frac{1}{\sqrt{c-a}}\left(\frac{(\sin\theta - i\cos\theta)\sqrt{(z_i-a)(z_i-c)}}{c-z_i}\right. \\ & +\frac{(\sin\theta + i\cos\theta)\bar{z}_i(z_i-\bar{z}_i)}{(c-\bar{z}_i)\sqrt{(\bar{z}_i-a)(\bar{z}_i-c)}} + \frac{(\sin\theta - i\cos\theta)\sqrt{(\bar{z}_i-a)(\bar{z}_i-c)}}{c-\bar{z}_i} \\ & \left.+\frac{(\sin\theta + i\cos\theta)(z_i-\bar{z}_i)\sqrt{(\bar{z}_i-a)(\bar{z}_i-c)}}{(c-\bar{z}_i)^2}\right), \end{aligned} \tag{27}$$

Referring to Bobylev et al. [7] and Morozov et al. [38], when the direction of crack growth is perpendicular to the external force, the SIFs at the crack tip a can be written as

$$K_I = K_I^{\sigma} + K_I^q + K_I^d + K_I^b, \tag{28}$$

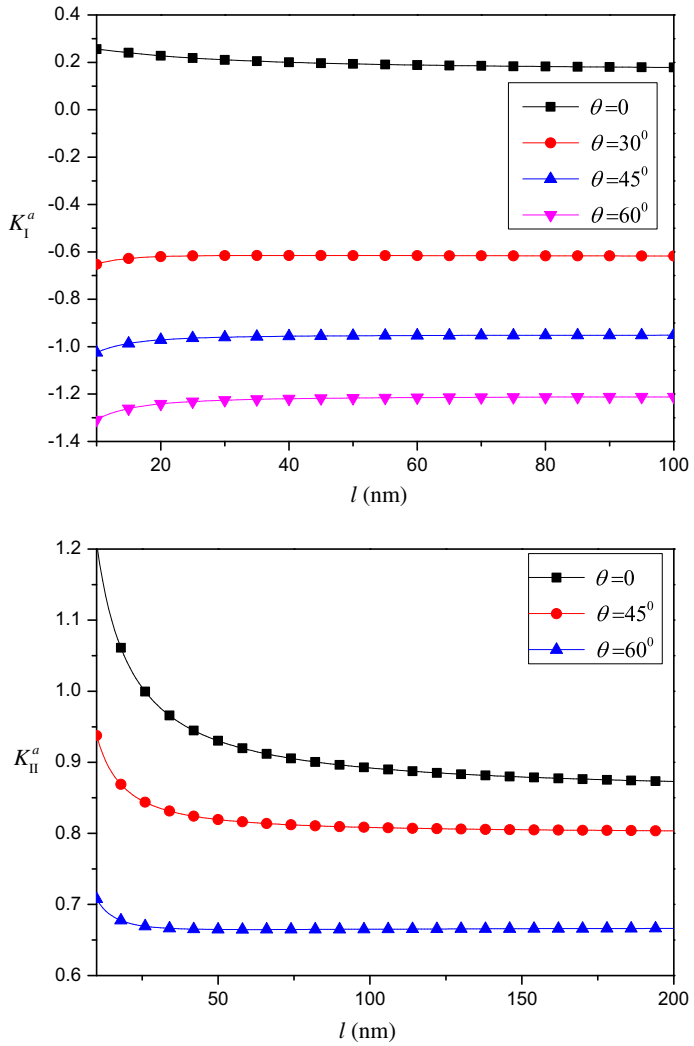

Fig. 8 Dependence of the normalized SIFs K_1^a and K_{II}^a on the crack length l with different θ ($\alpha = \pi/3$, ω=$\pi/72$, $\theta_0 = 10°$, $\theta_1 = 0°$, $d = 15$ nm and $s = 3$ nm)

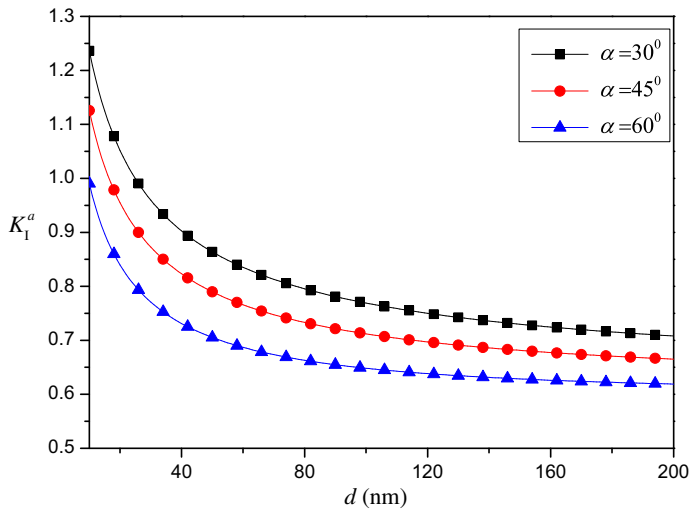

Fig. 9 Dependence of the normalized SIFs K_I^a on the twin size d with different α ($\theta = \pi/6$, ω=$\pi/72$, $r_1 = 0.1$ nm, $\theta_0 = 10°$, $\theta_1 = 0°$ and $s = 3$ nm)

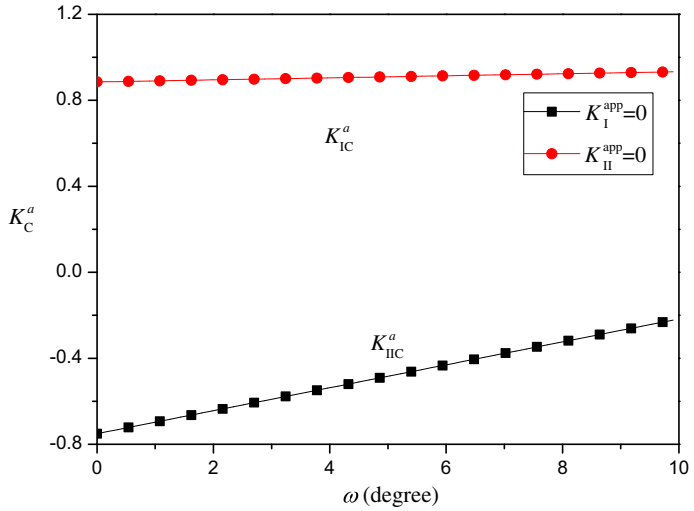

Fig. 10 Dependence of the normalized SIFs K_I^a and K_{II}^a on the disclination strength ω ($\theta = \pi/6$, $\alpha = \pi/3$, $\theta_1 = 0°$, $d = 15$ nm and $s = 3$ nm)

$$K_{\mathrm{II}} = K_{\mathrm{II}}^q + K_{\mathrm{II}}^d + K_{\mathrm{II}}^b. \tag{29}$$

Here, K_{I}^σ is the SIF induced by the external stress, K_{I}^q and K_{II}^q are the SIFs created by the disclination quadrupole located near the crack tip, K_{I}^d and K_{II}^d are the SIFs produced by the first dislocation emitted from the crack tip, and K_{I}^b and K_{II}^b are the SIFs created by the dislocation pileup at the twin boundary.

Utilizing the expressions of the SIFs K_{I} and K_{II}, the shielding and the anti-shielding effect on the crack tip a can be analyzed. For simplicity, the normalized SIFs are defined as $K_{\mathrm{I}}^a = K_{\mathrm{I}}/(\mu\sqrt{b})$ and $K_{\mathrm{II}}^a = K_{\mathrm{II}}/(\mu\sqrt{b})$. The normalized SIFs K_{I}^a and K_{II}^a versus the crack length l with different emission angle θ are depicted in Fig. 8. It can be seen that the crack length has only a slight influence on the mode I shielding/anti-shielding effect on the crack tip, but the emission angle has a significant effect on that. When $\theta = 0°$, there is an anti-shielding effect on the crack tip; however, when $\theta > 0°$, there is a shielding effect on the crack tip which increases dramatically with increasing emission angle. The mode II anti-shielding effect on the crack tip decreases with increasing crack length and also decreases with the increasing emission angle.

The dependence of the normalized SIFs K_{I}^a on the twin size d with different twin orientation α is depicted in Fig. 9. It shows that the mode I anti-shielding effect on the crack tip decreases with the increment of grain size and the twin orientation α, which is in agreement with Fig. 5. The dependence of the normalized SIFs K_{I}^a and K_{II}^a on the disclination strength is shown in Fig. 10. It can be found that with increasing disclination strength, the mode I anti-shielding effect on the crack tip increases while the mode II shielding effect decreases.

6 Conclusions

In this paper, the interaction of the twin and the dislocation pileup at the twin boundary with the crack is investigated by the complex variable method. The critical SIFs for the first dislocation emission are calculated. The effects of the crack length, twin size, disclination strength and twin location on the critical SIFs are investigated. Meanwhile, the shielding/anti-shielding effects of the twin, the dislocation pileup at the twin boundary and the first dislocation emitted from the crack tip on the crack tip a are theoretically analyzed. Some important conclusions are summarized as follows.

Both the twin and the dislocation pileup at the twin boundary release the high stresses near the crack tip and therefor enhance the critical SIFs (caused by the applied loadings) for the dislocation emission. The strength of the twin is higher, the edge dislocation is more difficult to emit from the crack tip. The suppressive effect induced by the dislocation pileup at the twin boundary is much stronger than that by the twin. In addition, the twin has great influence on the most probable angle for dislocation emission.

When the twin and the dislocation pileup at the twin boundary are certain, the mode II loadings emit the dislocations from the crack tip easier than the mode I loadings.

The location of the twin also has a significant influence on the dislocation emission from the crack tip. Under certain circumstances, there is a best twin position which can make the dislocation emission easiest.

The crack length has only a slight influence on the mode I shielding/anti-shielding effect on the crack tip, but the emission angle has a significant effect on that. When $\theta = 0°$, there is an anti-shielding effect on the crack tip; however, when $\theta > 0°$, there is a shielding effect, and it increases dramatically with increasing of emission angle.

Acknowledgements The authors would like to deeply appreciate the support from the National Natural Science Foundation of China (11372103, 11572118 and 11602080), the Hunan Provincial Science Fund for Distinguished Young Scholars (2015JJ1006), the folk Ying-Tong Education Foundation, China (141005).

References

1. Aifantis, E.C.: Deformation and failure of bulk nanograined and UFG materials. Mater. Sci. Eng. A **503**(1–2), 190–197 (2009)
2. Barai, p, Weng, G.J.: Mechanics of very fine-grained nanocrystalline materials with contributions from grain interior, GB zone, and grain boundary sliding. Int. J. Plast. **25**(12), 2410–2434 (2009)
3. Bobylev, S.V., Mukherjee, A.K., Ovid'ko, I.A.: Emission of partial dislocations from amorphous intergranular boundaries in deformed nanocrystalline ceramics. Scr. Mater. **60**(1), 36–39 (2009)
4. Koch, C.C.: Structural nanocrystalline materials: an overview. J. Mater. Sci. **42**(5), 1403–1414 (2007)
5. Ovid'ko, I.A., Sheinerman, A.G.: Special strain hardening mechanism and nanocrack generation in nanocrystalline materials. Appl. Phys. Lett. **90**(17), 171927 (2007)
6. Kolesnikova, A.L., Ovid'ko, I.A., Fedorov, A.A.: Local migration of grain boundaries in polycrystalline materials under plastic deformation conditions. Tech. Phys. Lett. **29**(6), 488–490 (2003)
7. Vergazov, A.N., Likhachev, V.A., Rybin, V.V., Solomko, YuV: Fragmented structure peculiarities in molybdenum alloys with different mechanical properties. Fiz. Met. Metalloved. **43**(1), 70–75 (1977)
8. Rybin, V.V.: High plastic strains and fracture of metals. Metallurgiya, Moscow (1986)
9. Bobylev, S.V., Mukherjee, A.K., Ovid'ko, I.A., Sheinerman, A.G.: Effects of intergrain sliding on crack growth in nanocrystalline materials. Int. J. Plast. **26**(11), 1629–1644 (2010)
10. Ovid'ko, I.A., Sheinerman, A.G.: Deformation twinning through nanoscale ideal shears in nano-and polycrystalline materials at ultra high stresses. Rev. Adv. Mater. Sci. **27**(2), 189–194 (2011)
11. Zhang, T.Y., Li, J.C.M.: Interaction of an edge dislocation with an interfacial crack. J. Appl. Phys. **72**(6), 2215–2226 (1992)
12. Doiphode, R.L., Murty, S.V.S.N., Prabhu, N., Kashyap, B.P.: Grain growth in caliber rolled Mg-3Al-1Zn alloy and its effect on hardness. J. Magnes. Alloys **3**(4), 322–329 (2015)
13. Jiang, L., Bi, G., Wang, G., Jiang, Q., Lian, J., Jiang, Z.: Strain-hardening and warm deformation behaviors of extruded Mg–Sn–Yb alloy sheet. J. Magnes. Alloys **2**(2), 116–123 (2014)
14. Singarapu, U., Adepu, K., Arumalle, S.R.: Influence of tool material and rotational speed on mechanical properties of friction stir welded AZ31B magnesium alloy. J. Magnes. Alloys **3**(4), 335–344 (2015)
15. Zhang, R.Y., Daymond, M.R., Holt, R.A.: A finite element model of deformation twinning in zirconium. Mater. Sci. Eng. A **473**(1–2), 139–146 (2008)
16. Romanov, A.E., Vladimirov, V.I.: Disclinations in crystalline solids. In: Nabarro, F.R.N. (ed.) Dislocations in Solids, vol. 9, pp. 191–402. North-Holland, Amesterdam (1992)
17. Feng, H., Fang, Q.H., Liu, B., Liu, Y., Liu, Y.W., Wen, P.H.: Nucleation and growth mechanisms of nanoscale deformation twins in hexagonal-close-packed metal magnesium. Mech. Mater. **109**, 26–33 (2017)
18. Hirth, J.P., Lorth, J.: Theory of Dislocations, 2nd edn. John-wiley, New York (1964)
19. Lu, L., Schwaiger, R., Shan, Z.W., Dao, M., Lu, K., Suresh, S.: Nano-sized twins induce high rate sensitivity of flow stress pure copper. Acta Mater. **53**(7), 2169–2179 (2005)
20. Lu, L., Dao, M., Zhu, T., Li, J.: Size dependence of rate-controlling deformation mechanisms in nanotwinned copper. Scr. Mater. **60**(12), 1062–1066 (2009)
21. Lu, L., You, Z.S., Lu, K.: Work hardening of polycrystalline Cu with nanoscale twins. Scr. Mater. **66**(11), 837–842 (2012)
22. Muskhelishvili, N.L., Radok, J.R.M.: Some Basic Problems of the Mathematical Theory of Elasticity: Fundamental Equations, Plane Theory of Elasticity, Torsion and Bending. Noordhoof, Groningen (1953)
23. Gutkin, M.Y., Ovid'ko, I.A., Skiba, N.V.: Crack-stimulated generation of deformation twins in nanocrystalline metals and ceramics. Philos. Mag. **88**(8), 1137–1151 (2008)
24. Ovid'ko, I.A.: Review on fracture processes in nanocrystalline materials. J. Mater. Sci. **42**(5), 1694–1708 (2007)
25. Feng, H., Fang, Q.H., Liu, Y.W., Chen, C.P.: Nanoscale rotational deformation effect on dislocation emission from an elliptically blunted crack tip in nanocrystalline materials. Int. J. Solids Struct. **51**(2), 352–358 (2014)
26. Fang, Q.H., Feng, H., Liu, Y.W., Lin, S., Zhang, N.: Special rotational deformation effect on the emission of dislocations from a crack tip in deformed nanocrystalline solids. Int. J. Solids Struct. **49**(11–12), 1406–1412 (2012)
27. Fang, Q.H., Liu, Y.W., Jang, C.P.: Edge dislocation interacting with an interfacial crack along a circular inhomogeneity. Int. J. Solids Struct. **40**(21), 5781–5797 (2003)
28. Ovid'ko, I.A., Sheinerman, A.G., Alfantis, E.C.: Effect of cooperative grain boundary sliding and migration on crack growth in nanocrystalline solids. Acta Mater. **59**(12), 5023–5031 (2011)
29. Zhang, S., Zhou, J.Q., Wang, L., Liu, H.X., Dong, S.H.: Crack nucleation due to dislocation pile-ups at twin boundary-grain boundary intersections. Mater. Sci. Eng. A **632**, 78–81 (2015)

30. Muskhelishvili, N.L.: Some Basic Problems of Mathematical Theory of Elasticity. Noordhoff, Leyden (1975)
31. Fang, Q.H., Liu, Y.W., Jin, B., Wen, P.H.: Effect of interface stressed on the image force and stability of an edge dislocation inside a nanoscale cylindrical inclusion. Int. J. Solids Struct. **46**(6), 1413–1422 (2009)
32. Feng, H., Fang, Q.H., Zhang, L.C., Liu, Y.W.: Effect of cooperative grain boundary sliding and migration on emission of dislocations from a crack tip in nanocrystalline materials. Mech. Mater. **61**, 39–48 (2013)
33. Asaro, R.J., Suresh, S.: Mechanistic models for the activation volume and rate sensitivity in metals with nanocrystalline grains and nano-scale twins. Acta Mater. **53**(12), 4825–4838 (2005)
34. Zhu, B., Asaro, J.R., Krysl, P., Bailey, R.: Transition of deformation mechanisms and its connection to grain size distribution in nanocrystalline metals. Acta Mater. **53**(18), 4825–4838 (2005)
35. Neuber, H.: Theory of Notch Stresses. Springer, Berlin (1958)
36. Irwin, G.R.: Analysis of stresses and strains near the end of a crack traversing a plate. J. Appl. Mech. **24**, 361–364 (1957)
37. Rice, J.R., Thomson, R.: Ductile versus brittle behavior of crystals. Philos. Mag. **29**(1), 73–79
38. Morozov, N.F., Ovid'ko, I.A., Sheinerman, A.G., Aifantis, E.C.: Special rotational deformation as a toughening mechanism in nanocrystalline solids. J. Mech. Phys. Solids **58**(8), 1088–1099 (2010)
39. Huang, M.X., Li, Z.H.: Dislocation emission criterion from a blunt crack tip. J. Mech. Phys. Solids **52**(9), 1991–2003 (2004)
40. Fang, Q.H., Liu, Y.W., Jiang, C.P., Li, B.: Interaction of a wedge disclination dipole with interfacial cracks. Eng. Fract. Mech. **73**(9), 1235–1248 (2006)
41. Zhang, T.Y., Li, J.C.M.: Image forces and shielding effects of an edge dislocation near a finite length crack. Acta Metall. Mater. **39**(11), 2739–2744 (1991)
42. Demkowicz, M.J., Argon, A.S., Farkas, D., Frary, M.: Simulation of plasticity in nanocrystalline silicon. Philos. Mag. **87**(28), 4253–4271 (2007)